

ation from a cofactor with acetylating activity to sustain IFN- γ synthesis in T_H1 cells. The precise biochemical nature of the interactions and the actual targets of acetylation are being investigated (22).

Our results prompt reexamination of how the identity of the T_H1 lineage is specified. Upon stimulation, naïve cells activate T-bet, which coordinates a program of autoinduction, chromatin remodeling of IFN- γ alleles, and IL-12R β 2 expression. STAT4 is not essential in T-bet induction and is not required to aid T-bet in inducing the T_H1 identity. This appears to place T-bet upstream of the STAT4 pathway, not by acting on the *Stat4* gene itself, but by specifying that a cell stably expressing T-bet (and capable of reiterating IFN- γ) has the ability to activate STAT4 (17). STAT4 nevertheless confers benefits that are essential to cell-mediated immunity, perhaps by ensuring that some T_H1 progeny will undergo sufficient cell divisions to emigrate from lymph nodes (28, 29) and, through genetic interactions with CBP and IL-18, arrive at tissue maximally armed.

Although Gata-3 can autoinduce itself and remodel the IL-4 locus without assistance from STAT6 (7), neither selection nor enhancement of IL-4 gene expression have yet been implicated as critical roles for STAT6 (4, 7–9). In addition to their positive effects on T_H2 and T_H1 development, IL-4 (Fig. 1) and IL-12 (7, 30), acting via STAT proteins, potentially suppress induction of T-bet and Gata-3, thereby limiting differentiation of T_H1 and T_H2 subsets, respectively. It is, therefore, likely that parallel pathways of instruction, in which cytokines repress or induce activators of specific lineages, can coexist with mechanisms of selection.

Phorbol 12-myristate 13-acetate (PMA) (50 ng/ml) and ionomycin (500 ng/ml) were used for restimulation of less than 6 hours. PMA (1 ng/ml) and ionomycin (500 ng/ml) were used for restimulation of greater than 12 hours. BALB/c *Stat4*^{-/-} (12), C57BL/6 *Irfng*^{+/-} (17), and wild-type mice were obtained from the Jackson Laboratories. C57BL/6 *Cbp*^{+/-} mice were generated as described (26). All animal work was performed in accordance with University of Pennsylvania guidelines.

For retroviral transduction, polymerase chain reaction (PCR) was used to add a consensus Kozak sequence upstream of the T-bet start ATG, and the cDNA was cloned into vector MigRI upstream of an internal ribosomal entry sequence followed by GFP cDNA. Transfection of a packaging cell line was performed as described (17). CD8-depleted splenocytes were stimulated in the presence of mAb against CD3 (0.4 μ g/ml), mAb against CD28 (0.5 μ g/ml), rIL-2 (20 U/ml), and additional cytokines as specified. After 24 hours, cells were harvested, resuspended in viral supernatant containing polybrene (8 μ g/ml), and centrifuged at 6000g for 90 min at 25°C. After centrifugation, cells were resuspended in media containing rIL-2 (40 U/ml) and their initial cytokine conditions.

For DNase I hypersensitivity analysis, *Stat4*^{-/-} cells were stimulated in rIL-4 and infected with T-bet or control retrovirus. GFP-positive cells were sorted using a MoFlo cytometer (Cytomation) 2 days after infection. DNase I digestions were performed on isolated nuclei, as described (17). Briefly, nuclei were incubated for 15 min at 37°C with DNase I (0, 0.25, or 0.5 μ g/ml) at a density of 4×10^7 nuclei/ml. Analysis of the IFN- γ locus was performed as described (27). Briefly, genomic DNA was digested overnight with Bam HI and resolved through 0.8% agarose before transfer to nylon membranes. Blots

were probed with a 410-bp fragment of IFN- γ exon 4 generated by PCR using the following primers: sense GCGCAAGCATTC AATGAGCTCATCCGAG and antisense GAGTTCAGTCAGCCGCTGGCTGTGTC. All experiments in this report were performed at least twice.

15. S. J. Simpson *et al.*, *J. Exp. Med.* **187**, 1225 (1998).
16. R. A. Seder, W. E. Paul, M. M. Davis, B. Fazekas de St. Groth, *J. Exp. Med.* **176**, 1091 (1992).
17. Supplementary material is available at www.sciencemag.org/cgi/content/full/292/5523/1907/DC1.
18. G. A. Hollander *et al.*, *Science* **279**, 2118 (1998).
19. M. Bix, R. M. Locksley, *Science* **281**, 1352 (1998).
20. I. Riviere, M. J. Sunshine, D. R. Littman, *Immunity* **9**, 217 (1998).
21. S. Agarwal, A. Rao, *Immunity* **9**, 765 (1998).
22. A. C. Mullen, F. A. High, A. S. Hutchins, S. L. Reiner, unpublished observations.
23. J. J. Bird *et al.*, *Immunity* **9**, 229 (1998).
24. W. X. Zhang, S. Y. Yang, *Genomics* **70**, 41 (2000).
25. E. Korzus *et al.*, *Science* **279**, 703 (1998).
26. A. L. Kung *et al.*, *Genes Dev.* **14**, 272 (2000).
27. J. Yang, T. L. Murphy, W. Ouyang, K. M. Murphy, *Eur. J. Immunol.* **29**, 548 (1999).
28. F. Sallusto, D. Lenig, R. Forster, M. Lipp, A. Lanzavecchia, *Nature* **401**, 708 (1999).
29. A. Langenkamp, M. Messi, A. Lanzavecchia, F. Sallusto, *Nature Immunol.* **1**, 311 (2000).
30. W. Ouyang *et al.*, *Immunity* **9**, 745 (1998).
31. We are grateful to P. Scott, C. Hunter, C. Thompson, and G. Koretzky for critical comments, W. Pear and L. Xu for advice and reagents, and W. DeMuth for cell sorting. This work was supported by the NIH (AI-42370 to S.L.R. and EY-07131 to A.C.M.).

13 February 2001; accepted 8 May 2001

A p53 Amino-Terminal Nuclear Export Signal Inhibited by DNA Damage–Induced Phosphorylation

Yanping Zhang* and Yue Xiong†

The p53 protein is present in low amounts in normally growing cells and is activated in response to physiological insults. MDM2 regulates p53 either through inhibiting p53's transactivating function in the nucleus or by targeting p53 degradation in the cytoplasm. We identified a previously unknown nuclear export signal (NES) in the amino terminus of p53, spanning residues 11 to 27 and containing two serine residues phosphorylated after DNA damage, which was required for p53 nuclear export in collaboration with the carboxyl-terminal NES. Serine-15–phosphorylated p53 induced by ultraviolet irradiation was not exported. Thus, DNA damage–induced phosphorylation may achieve optimal p53 activation by inhibiting both MDM2 binding to, and the nuclear export of, p53.

The gene encoding p53 mediates a major tumor suppression pathway that is frequently altered in human cancers (1). p53 is inhibited

during normal cell growth by MDM2, a proto-oncogene discovered by its genomic amplification on a murine double minute chromosome, through either ubiquitin-dependent p53 degradation in the cytoplasm (2) or repression of p53's transcriptional activity in the nucleus (3, 4). p53 is activated after DNA damage through p53 phosphorylation (5, 6), or in response to oncogenic insults by the activation of ARF, a tumor suppressor encoded by the alternative reading frame of the INK4a locus that is frequently altered in human cancers (7). Blocking p53 nuclear export

Lineberger Comprehensive Cancer Center, Department of Biochemistry and Biophysics, and Program in Molecular Biology and Biotechnology, University of North Carolina at Chapel Hill, NC 27599–7295, USA.

*Present address: Department of Molecular and Cellular Oncology, University of Texas, M. D. Anderson Cancer Center, Houston, TX 77030, USA.

†To whom correspondence should be addressed. E-mail: yxiong@email.unc.edu

References and Notes

1. T. R. Mosmann, H. Cherwinski, M. W. Bond, M. A. Giedlin, R. L. Coffman, *J. Immunol.* **136**, 2348 (1986).
2. K. M. Murphy *et al.*, *Annu. Rev. Immunol.* **18**, 451 (2000).
3. R. L. Coffman, S. L. Reiner, *Science* **284**, 1283 (1999).
4. J. D. Farrar *et al.*, *J. Exp. Med.* **193**, 643 (2001).
5. S. J. Szabo *et al.*, *Cell* **100**, 655 (2000).
6. W. Zheng, R. A. Flavell, *Cell* **89**, 587 (1997).
7. W. Ouyang *et al.*, *Immunity* **12**, 27 (2000).
8. H. Kurata, H. J. Lee, A. O'Garra, N. Arai, *Immunity* **11**, 677 (1999).
9. J. L. Grogan *et al.*, *Immunity* **14**, 205 (2001).
10. M. H. Kaplan, A. L. Wurster, M. J. Grusby, *J. Exp. Med.* **188**, 1191 (1998).
11. F. D. Finkelman *et al.*, *J. Immunol.* **164**, 2303 (2000).
12. M. H. Kaplan, Y. L. Sun, T. Hoey, M. J. Grusby, *Nature* **382**, 174 (1996).
13. M. H. Kaplan, U. Schindler, S. T. Smiley, M. J. Grusby, *Immunity* **4**, 313 (1996).
14. Cell stimulation, CFSE labeling, intracellular cytokine staining, and flow cytometry were performed as previously described (23). Stimulation used CD8-depleted splenocytes from naïve mice (2×10^6 cells/ml), with monoclonal antibody (mAb) against CD3 (0.1 μ g/ml, all Pharmingen unless indicated), mAb against CD28 (0.5 μ g/ml), human recombinant IL-2 (rIL-2, 10 U/ml, LifeSciences), and, if indicated, rIL-4 (5 U/ml, Roche), rIL-12 (2.5 ng/ml), rIL-18 (50 ng/ml, R&D Systems); antibodies against IL-4 (11B11, 10 μ g/ml), IL-12 (1 μ g/ml), and IL-18 (2 ng/ml, R&D Systems).

REPORTS

leads to p53 stabilization and activation (8, 9), and ARF stabilizes p53, in part, by blocking the nuclear export of both p53 and MDM2 (10, 11), underscoring the importance of nuclear export in regulating p53 stability.

The mechanism governing p53 nuclear export remains unclear, and three competing models have been proposed (12). MDM2 may bind p53 in the nucleus and shuttle it to the cytoplasm (8, 13), p53 may use a COOH-terminal–located nuclear export signal (NES) to mediate its own nuclear export (14), or MDM2 could ubiquitinate p53 in the nucleus to promote its nuclear export (15, 16). To clarify the role of MDM2 in p53 nuclear export and discriminate between these models, we first examined the sensitivity to MDM2-mediated degradation and nuclear export of p53 harboring either L14Q/F19S (Leu¹⁴ → Gln; Phe¹⁹ → Ser) or L22Q/W23S (Leu²² → Gln; Trp²³ → Ser) mutations (17). Consistent with previous reports (2), both p53^{L14Q/F19S} and p53^{L22Q/W23S} were resistant to degradation by HDM2 (human homolog of MDM2) (Fig. 1A). The inhibition of HDM2-mediated p53 degradation by these mutations could not be attributed to the loss of p53 transcriptional activity, because a mutation in the sequence-specific DNA binding

domain, R273H (Arg²⁷³ → His), which also abolishes p53 transcriptional activity, had no detectable effect on p53 stability (18). Despite containing the intact NES in the COOH-terminal region (14), both p53^{L14Q/F19S} and p53^{L22Q/W23S} exhibited substantially decreased nuclear export activity, from 73% with wild-type (WT) p53 to 23% and 15%, with the two mutants, respectively (Fig. 1, B and C). The transcriptionally inactive p53^{R273H} was exported at an efficiency indistinguishable from that of WT p53 (Fig. 1B). Thus, the COOH-terminal–located NES was required, but was not sufficient, for p53 nuclear export. This result is different from a previous report of normal nuclear export of a p53^{L22Q/W23S}-green fluorescent protein (GFP) fusion (14). Several experimental differences in that study could have contributed to the discrepancy. These include the following, a four times longer cell fusion period, which would result in prolonged protein export; the electroporation of 10 times more plasmid DNA, which would result in a higher level of p53 protein; and the attachment of a GFP moiety that might have increased cytoplasmic retention of p53^{L22Q/W23S}-GFP, which would have then entered the mouse nuclei in the heterokaryons and scored as

positive nuclear export. Supporting the idea that the inhibitory effect of the L22Q/W23S mutation on p53 export may be reduced or even masked by the overproduction of p53, endogenous p53^{L22Q/W23S} protein produced by a knock-in strategy that was expressed at a lower level is more completely blocked from nuclear export and accumulates to very high levels in the nucleus [(19), Web fig. 1 (20)], providing *in vivo* evidence for the disruption of p53 nuclear export by L22Q/W23S mutations.

Blockage of p53 nuclear export by the L14Q/F19S and the L22Q/W23S mutations could be attributed to the disruption of p53-MDM2 association if MDM2 shuttled p53 out of the nucleus (10) or if MDM2 was required for p53 nuclear ubiquitination and its subsequent export (15, 16). Alternatively, it could be attributed to an intrinsic property of the NH₂-terminal domain of p53. We carried out a series of heterokaryon assays to determine if p53 nuclear export was dependent on MDM2. After examining a large number of heterokaryons, we did not observe apparent differences in p53 nuclear export efficiency in the absence of HDM2 or in the presence of high levels of HDM2 [Web fig. 2 (20)]. To exclude the possibility that

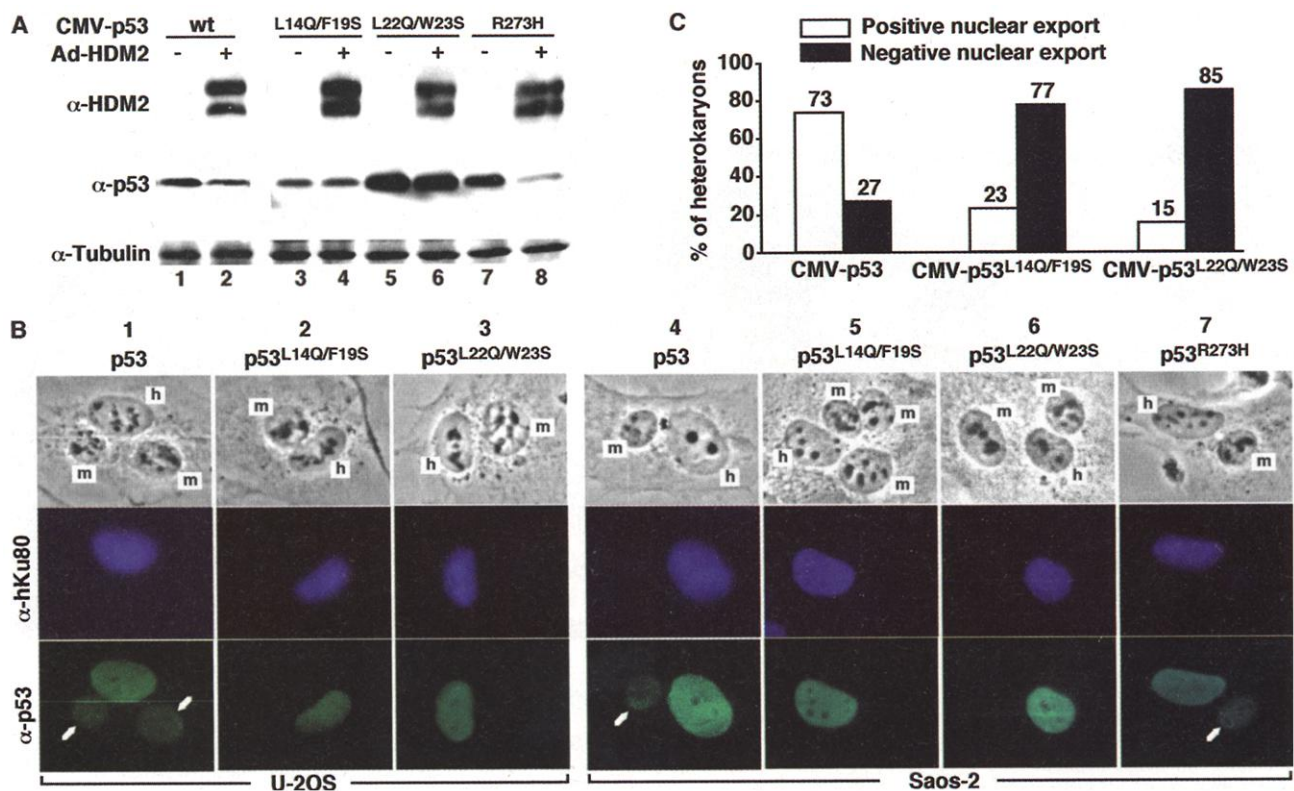


Fig. 1. p53 nuclear export is impaired by mutations in the NH₂-terminal domain. (A) Saos-2 cells were infected with Ad-HDM2 and transfected with individual plasmids expressing the indicated p53 protein. Whole-cell lysates from each infected-transfected cell population were separated by SDS-polyacrylamide gel electrophoresis and immunoblotted with antibodies to HDM2 and p53. (B) Human Saos-2 and U-2OS cells were transfected with plasmid DNA expressing the indicated p53 proteins. Twenty hours after

transfection, cells were fused with MDM2^{-/-}-p53^{-/-} MEF cells while de novo protein synthesis was inhibited. Forty-five minutes after fusion, cells were fixed and stained with the indicated antibodies. Arrows indicate positive p53 nuclear export. Nuclei of human (h) or mouse (m) origin are indicated in the phase-contrast images. (C) Fifty heterokaryons were counted from each transfection. The appearance of p53 in the mouse (Ku-negative) nuclei was scored as positive p53 nuclear export.

REPORTS

trace amounts of HDM2 in the Saos-2 cells might have traveled to p53^{-/-}-MDM2^{-/-} mouse embryo fibroblasts (MEFs) and promoted p53 export, we performed a similar heterokaryon assay in which p53^{-/-}-MDM2^{-/-} MEFs were first infected with p53-expressing adenoviruses and then fused with Saos-2 cells that had been infected with ARF-expressing adenoviruses to block MDM2 export (10, 11). In these experiments, p53 shuttled from p53^{-/-}-MDM2^{-/-} MEFs to ARF-overexpressing Saos-2 cells in a majority (76%) of the heterokaryons examined (Fig. 2, A and C). In a separate experiment, p53 was expressed in one set of p53^{-/-}-MDM2^{-/-} MEFs, and then fused with another set of p53^{-/-}-MDM2^{-/-} MEFs that had been infected with adenovirus expressing hARF (Ad-hARF) and identified by an antibody specific to human, but not mouse, ARF. In a majority (84%) of the heterokaryons formed by fusion of ARF-negative (Ad-p53 infected) and ARF-positive (uninfected) p53^{-/-}-MDM2^{-/-} MEFs, active p53 nuclear export was observed (Fig. 2, B and C). The efficiency of p53 nuclear-cytoplasmic shuttling between two murine nuclei through the murine cytoplasm is comparable to that seen between human and mouse nuclei through a mixed human/mouse cytoplasm. Thus, p53 nuclear export was not dependent on the presence of MDM2, and impaired p53 nuclear export by the L14Q/F19S and L22Q/W23S

mutations is probably caused by a mechanism other than the disruption of p53-MDM2 association. The ability of p53 to export independently of MDM2 does not exclude the possibility that p53 nuclear export may be affected by the function of MDM2.

The NH₂-terminal region of p53 contains two hydrophobic, leucine-rich stretches that resemble the chromosomal region maintenance 1 (CRM1)-dependent NESs found in several different proteins including MDM2 and p53 (Fig. 3A). The first leucine-rich stretch is highly conserved between human and mouse p53 (15 out of 17 residues are identical) whereas only 8 out of 18 residues in the second leucine-rich sequence are conserved. Notably, the L14Q/F19S and L22Q/W23S mutations each alter a highly conserved hydrophobic Leu residue shown to be critically important for NES function in cyclic adenosine 3', 5'-monophosphate (cAMP)-dependent protein kinase inhibitor (PKI) (21), HDM2 (8), and p53 (14). We attached both p53¹¹⁻²⁷ and p53³¹⁻⁴⁷ peptides to GFP and determined whether these leucine-rich motifs function as an autonomous NES. GFP distributes throughout both the nucleus and the cytosol, with slightly more accumulation in the nucleus (Fig. 3, B and C). Fusion of GFP with the NES from either HDM2 or the p53 COOH-terminus (p53^{NES}) resulted in evident nuclear exclusion of fluorescence in about two-thirds of the cells (Fig. 3, B and C),

confirming the nuclear export activity of both NESs. Attachment of the peptide from p53 residues 11 to 27 (p53^{NES}) to GFP generated clear nuclear exclusion of GFP in about two-thirds of the cells, an efficiency comparable with that of NESs from HDM2 and the p53 COOH-terminus. The nuclear exclusion of GFP by fusion with all three NESs is, however, incomplete, and nuclear fluorescence remains visible. This is probably due to the combination of weak NES activity [see Web fig. 3 for quantitative comparison (20)] and visualization of cells as a plane, as opposed to three-dimensionally, with the consequent inability to exclude cytoplasmic fluorescence surrounding the nucleus as non-nuclear signals. Fusion with the p53³¹⁻⁴⁷ peptide only weakly affected GFP distribution, and less than one-quarter of the GFP-positive cells exhibited a slight cytoplasmic accumulation of GFP. The significance of this weak nuclear export activity, if genuine, is difficult to assess and remains unclear at present. Inhibition of CRM1 by leptomycin B treatment reverted the nuclear exclusion of GFP fused with HDM2^{NES}, p53^{NES}, and p53^{NES} to that of GFP alone (Fig. 3, B and C), indicating that nuclear export by these three NESs was CRM1-dependent. L14Q/F19S and L22Q/W23S mutations prevented nuclear exclusion of p53^{NES}-GFP, reinforcing the functional importance of these hydrophobic residues and the authenticity of the

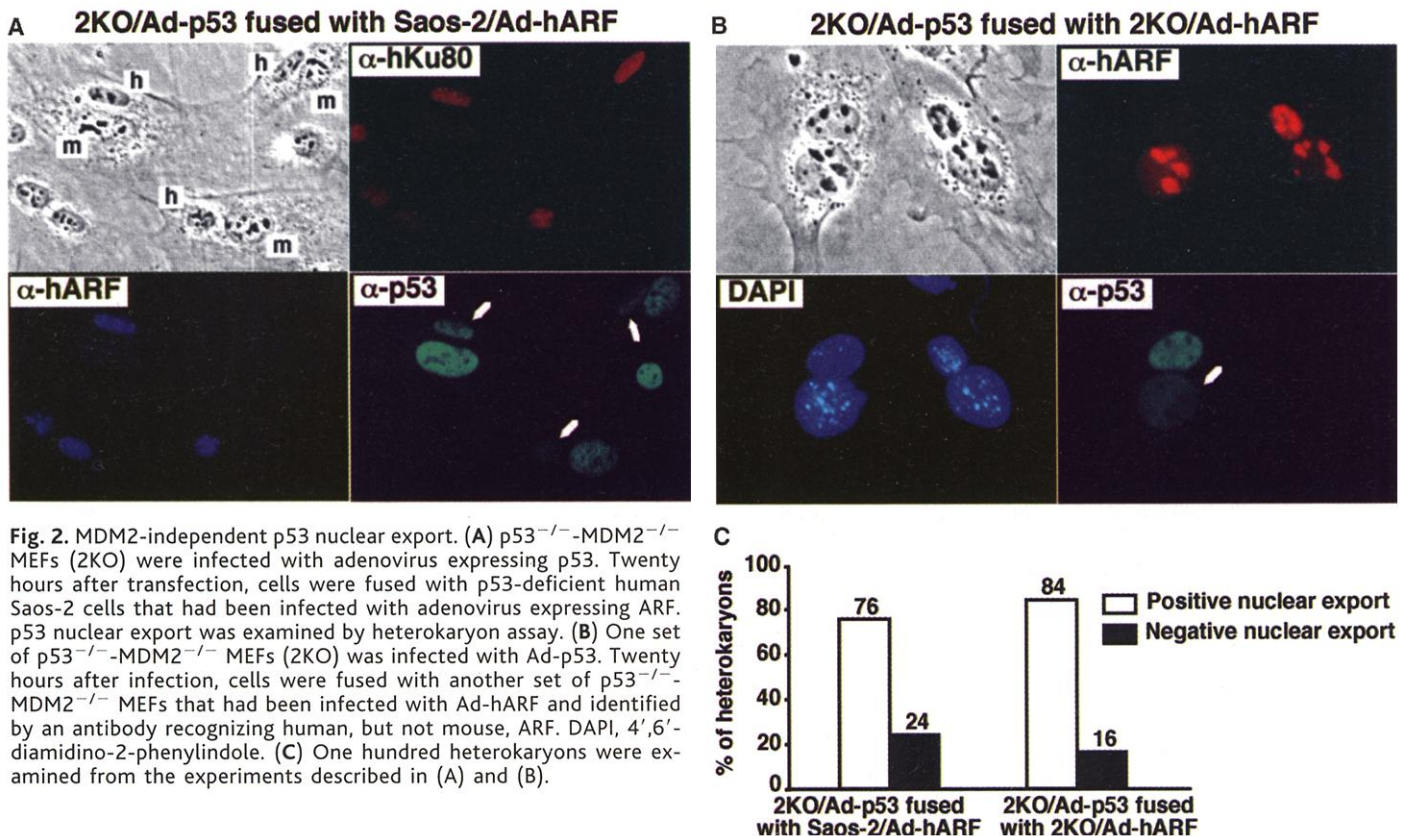


Fig. 2. MDM2-independent p53 nuclear export. (A) p53^{-/-}-MDM2^{-/-} MEFs (2KO) were infected with adenovirus expressing p53. Twenty hours after transfection, cells were fused with p53-deficient human Saos-2 cells that had been infected with adenovirus expressing ARF. p53 nuclear export was examined by heterokaryon assay. (B) One set of p53^{-/-}-MDM2^{-/-} MEFs (2KO) was infected with Ad-p53. Twenty hours after infection, cells were fused with another set of p53^{-/-}-MDM2^{-/-} MEFs that had been infected with Ad-hARF and identified by an antibody recognizing human, but not mouse, ARF. DAPI, 4',6'-diamidino-2-phenylindole. (C) One hundred heterokaryons were examined from the experiments described in (A) and (B).

REPORTS

p53 nNES. The nuclear export activity of the p53^{nNES}, as well as that of the p53^{cNES} and the PKI^{NES}, was not detectably affected by the high level of ARF expression (Fig. 3D). Thus, the NH₂-terminal domain of p53 appears to contain an autonomous NES that functions through the CRM1-dependent nuclear export pathway and is not dependent on MDM2.

The NH₂-terminal p53 NES contains two serine residues, Ser¹⁵ and Ser²⁰, adjacent to Leu¹⁴ and Leu²³. Phosphorylation of both Ser¹⁵ and Ser²⁰ by several DNA damage-activated p53 kinases has been linked to p53 stabilization and activation (22). A knock-in mutation at Ser¹⁸ of murine p53, which corresponds to Ser¹⁵ in human p53, delayed and reduced p53 accumulation and nearly completely abolished p21 accumulation in response to DNA damage (23). Substitution of both Ser¹⁵ and Ser²⁰ with alanine residues did

not cause any appreciable change in the nuclear and cytoplasmic distribution of fused GFP. However, the substitution of both Ser¹⁵ and Ser²⁰ with aspartic acid residues, which often mimic the charge of a phosphorylated serine, decreased nuclear export activity, as judged by the lack of visible nuclear exclusion of fused GFP and an increase in the ratio of nuclear to cytoplasmic fluorescence (Fig. 4A). To directly test the idea that phosphorylation at Ser¹⁵ and Ser²⁰ in p53 might impair the activity of the NH₂-terminal NES, we determined nucleo-cytoplasmic shuttling of phosphorylated p53 induced by DNA damage. Ad-p53-infected U-2OS cells were either left untreated or exposed to ultraviolet (UV) irradiation and then fused with Ad-ARF-infected Saos-2 cells. U-2OS/Saos-2 heterokaryons were identified by immunostaining with a mouse antibody to ARF. Nucleo-cytoplasmic shuttling of total or Ser¹⁵-

phosphorylated p53 was determined by using either a goat antibody against full-length human p53 (anti-full-length p53) or a rabbit antibody raised against a synthetic phospho-Ser¹⁵ p53 peptide (Fig. 4B). Anti-full-length p53 antibody detected high levels of p53 in almost all U-2OS cells (ARF negative) and lower amounts in the Saos-2 cells (ARF positive) present in the heterokaryons, but not in unfused Saos-2 cells, confirming the expression of p53 in U-2OS cells and its shuttling to the recipient Saos-2 cells. Anti-phospho-Ser¹⁵ p53 detected a considerable amount of p53 in UV-irradiated, but not in untreated, cells or UV-treated p53⁺ MEFs, confirming the specificity of the antibody in recognizing only the phosphorylated form of p53. Ser¹⁵-phosphorylated p53 was not detected in the recipient Saos-2 cells fused with UV-irradiated U-2OS cells in any of more than 30 heterokaryons that we examined. To deter-

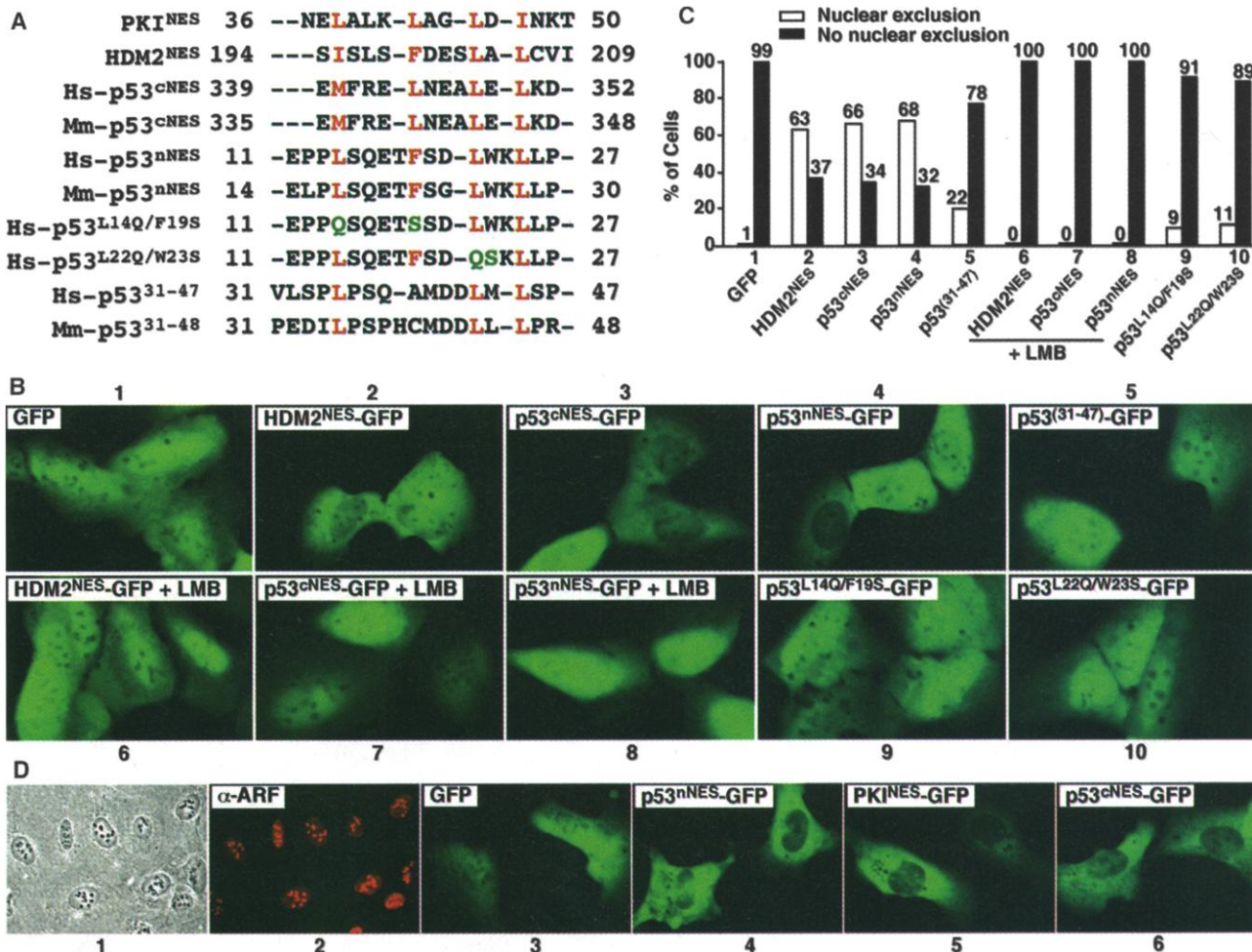


Fig. 3. The NH₂-terminal domain of p53 contains a functional NES. (A) Comparison of the NES sequences from human cAMP-dependent protein kinase inhibitor (Hs-PKI), HDM2, and the NH₂-terminally (nNES) and a COOH-terminally (cNES) located NESs from human (Hs) and mouse (Mm) p53 proteins. Highly conserved hydrophobic residues are shown in red and mutations are shown in green. Single-letter abbreviations for the amino acid residues are as follows: A, Ala; C, Cys; D, Asp; E, Glu; F, Phe; G, Gly; H, His; I, Ile; K, Lys; L, Leu; M, Met; N, Asn; P, Pro; Q, Gln; R, Arg; S, Ser; T, Thr; V, Val; W, Trp; and Y, Tyr. (B) Plasmids expressing naked

GFP and various GFP fusion proteins as indicated were transfected into U-2OS cells. Thirty-six hours after transfection, the subcellular localization of GFP was examined microscopically in live cells. (C) Cells with clear nuclear exclusion of GFP were scored as positive. More than 200 cells were counted for each sample. (D) MDM2-independent function of the p53 NH₂-terminal NES. U-2OS cells were first infected with Ad-ARF to block possible MDM2 nuclear export (panels 1 and 2). The cells were then transfected with the indicated plasmids, and the subcellular localization of GFP was examined microscopically in live cells (panels 3 to 6).

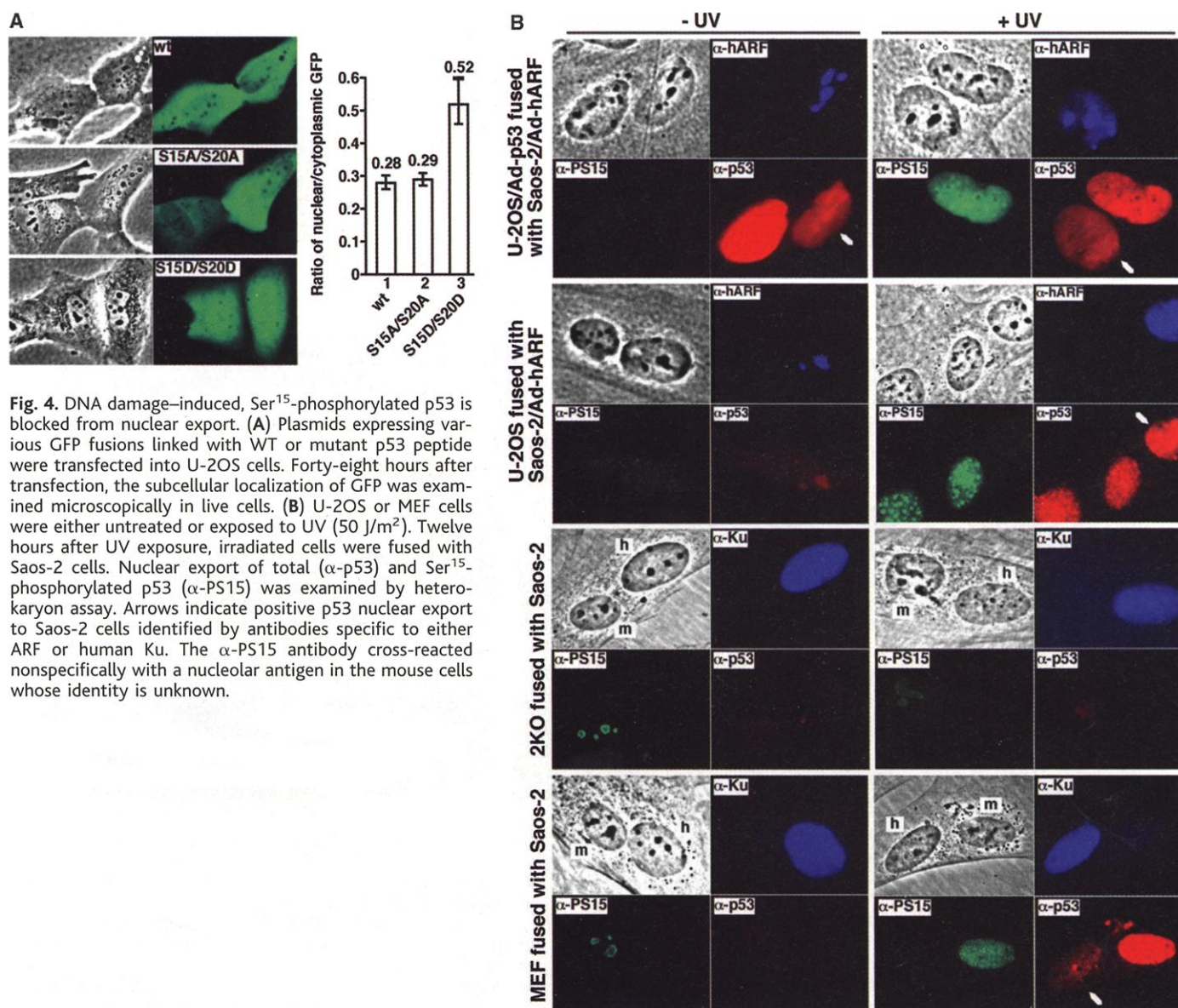
REPORTS

mine whether endogenously expressed, Ser¹⁵-phosphorylated p53 is similarly blocked from export. U-2OS cells were either left untreated or irradiated with UV and then fused with Saos-2 cells. Almost no p53 was detected in untreated U-2OS cells (Fig. 4B). After UV irradiation, there was a substantial increase in total and Ser¹⁵-phosphorylated p53. Ser¹⁵-phosphorylated p53 was localized mostly to speckles and exhibited a pattern distinct from that detected by anti–full-length p53, suggesting that phosphorylation of p53 is associated with or promotes a change of p53 subnuclear localization. Where there was active p53 nuclear export, as determined by the use of anti–full-length p53 antibody, no Ser¹⁵-p53 signal was detected in the recipient Saos-2 cells of more than 30 heterokaryons examined. UV irradiation similarly resulted in a substantial increase in total and Ser¹⁵-phosphorylated p53 in MEFs. A portion of

p53 detected by anti–full-length p53 was exported reproducibly at a lower level in MEFs than in U2OS cells, possibly resulting from more efficient p53 phosphorylation (thus blocking export) and a lower efficiency of anti–human p53 in recognizing mouse protein. Consistently, Ser¹⁵-phosphorylated p53 was completely blocked from nuclear export in more than 50 heterokaryons examined.

Our results reveal a previously unrecognized NES in the NH₂-terminal region of p53 that is required for the nuclear export of p53. The two separate NESs of p53 can functionally collaborate with each other and synergistically mediate protein nuclear export [Web fig. 3 (20)]. Having two separate NESs could provide cells with greater versatility in regulating p53 export. The carboxyl-terminal p53 NES is situated within the tetramerization domain, leading to the postulation that regulated p53 tet-

ramerization occludes this NES, thereby ensuring nuclear retention of the active DNA-binding form of p53 (14). The amino terminus of p53 contains several sites whose phosphorylation by various DNA damage-activated p53 kinases leads to p53 stabilization and activation (22). The inability of Ser¹⁵-phosphorylated p53 to undergo nuclear export suggests a previously unrecognized mechanism—inhibitory phosphorylation of a NES—for stabilizing and activating p53 in response to DNA damage. It remains to be determined whether phosphorylation at Ser¹⁵ alone is sufficient to inhibit p53 export or whether simultaneous phosphorylation at multiple residues, including Ser²⁰, is required. Phosphorylation at Ser¹⁵ and Ser²⁰ has been suggested to cause p53 stabilization by hindering p53-MDM2 binding (24). Because p53 can undergo active nuclear export in the absence



of MDM2 (14) (Fig. 2), inhibition of MDM2 binding, although preventing p53 degradation, would not block p53 nuclear export and thus would not efficiently accumulate p53 in the nucleus to allow maximal p53 activation. On the other hand, inhibiting p53 nuclear export without breaking its binding with MDM2, although causing the nuclear accumulation of p53, would not reach maximal p53 activation either because MDM2, in addition to its activity in promoting cytoplasmic p53 degradation, can also directly inhibit p53's transactivating activity in the nucleus (4). We suggest that DNA damage-induced phosphorylation may achieve optimal p53 activation through the additive and complementary action of both inhibiting MDM2 binding to, and the nuclear export of, p53.

References and Notes

1. A. J. Levine, *Cell* **88**, 323 (1997).
2. Y. Haupt, R. Maya, A. Kazaz, M. Oren, *Nature* **387**, 296 (1997); M. H. G. Kubbutat, S. N. Jones, K. H. Vousden, *Nature* **387**, 299 (1997); R. Honda, H. Tanaka, H. Yasuda, *FEBS Lett.* **420**, 25 (1997).
3. J. Momand, G. P. Zambetti, D. C. Olson, D. George, A. J. Levine, *Cell* **69**, 1237 (1992).
4. C. J. Thut, J. A. Goodrich, R. Tjian, *Genes Dev.* **11**, 1974 (1997).
5. L. J. Ko, C. Prives, *Genes Dev.* **10**, 1054 (1996).
6. M. Oren, *J. Biol. Chem.* **274**, 36031 (2000).
7. C. J. Sherr, *Genes Dev.* **12**, 2984 (1998).
8. J. Roth, M. Dobbstein, D. A. Freedman, T. Shenk, A. J. Levine, *EMBO J.* **17**, 554 (1998).
9. D. A. Freedman, A. J. Levine, *Mol. Cell. Biol.* **18**, 7288 (1998).
10. W. Tao, A. J. Levine, *Proc. Natl. Acad. Sci. U.S.A.* **96**, 6937 (1999).
11. Y. Zhang, Y. Xiong, *Mol. Cell* **3**, 579 (1999).
12. _____, *Cell Growth Differ.* **12**, 175 (2001).
13. W. Tao, A. J. Levine, *Proc. Natl. Acad. Sci. U.S.A.* **96**, 3077 (1999).
14. J. M. Stommel, et al., *EMBO J.* **18**, 1660 (1999).
15. S. D. Boyd, K. Y. Tsai, T. Jacks, *Nature Cell Biol.* **2**, 563 (2000).
16. R. K. Geyer, Z. K. Yu, C. G. Maki, *Nature Cell Biol.* **2**, 569 (2000).
17. J. Lin, J. Chen, A. J. Levine, *Genes Dev.* **8**, 1235 (1994).
18. Plasmids expressing WT p53, mutant p53^{L14Q/F195}, p53^{L22Q/W235}, and p53^{R273H} were provided by J. Chen. All other p53 mutants were generated by site-directed mutagenesis with a Quick-Change kit (Stratagene, La Jolla, CA) and verified by DNA sequencing. Cells, cell culture, and procedures for transfection, adenovirus infection, and immunoblotting are described in (25). Procedures for indirect immunofluorescence and heterokaryon assay are described in (17) except that the incubation time with primary anti-p53 was increased to overnight at 4°C to detect UV-induced p53 in MEFs. Fluorescence images were captured with a cooled charge-coupled device color digital camera (Diagnostic, model 2.2.0) and analyzed on a Macintosh computer with the public domain NIH Image program (version 1.61; available at <http://rsb.info.nih.gov/nih-image/>). Dilutions and sources of primary antibodies for indirect immunofluorescence are as follows: 0.2 µg/ml for mouse anti-MDM2 (clone SMP14, NeoMarkers, Fremont, CA), 0.04 µg/ml for rabbit anti-MDM2 (N-20, Santa Cruz Biotechnology, Santa Cruz, CA), 0.4 µg/ml (MEFs) or 0.2 µg/ml (other cells) for goat anti-p53 (sc-6243G, Santa Cruz), 1:5000 dilution for affinity-purified rabbit anti-Ser¹⁵-phospho-p53 (#9284, New England Biolabs, Beverly, MA), 0.4 µg/ml for mouse anti-ARF (clone 14P02, NeoMarkers), and 2 µg/ml for anti-Ku (p80, clone 111, NeoMarkers). All fluorochrome-conjugated secondary antibodies (Jackson Immuno-

Research Laboratories, West Grove, PA) are diluted to 5 µg/ml. For leptomycin B treatment, cells were treated with 5 ng/ml leptomycin B for 6 hours before cell fusion and/or fixation.

19. G. S. Jimenez, et al., *Nature Genet.* **26**, 37 (2000); C. Chao, et al., *EMBO J.* **19**, 4967 (2000).
20. Supplementary material available on Science online at www.sciencemag.org/cgi/content/full/292/5523/1910/DC1.
21. W. Wen, J. L. Meinkoth, R. Y. Tsien, S. S. Taylor, *Cell* **82**, 463 (1995).
22. A. J. Giaccia, M. B. Kastan, *Genes Dev.* **12**, 2973 (1998); C. Prives, *Cell* **95**, 5 (1998).
23. C. Chao, S. Saito, C. W. Anderson, E. Appella, Y. Xu, *Proc. Natl. Acad. Sci. U.S.A.* **97**, 11936 (2000).
24. S.-Y. Shieh, M. Ikeda, Y. Taya, C. Prives, *Cell* **91**, 325 (1997); N. H. Chehab, A. Malikzay, M. Appel, T. D. Halazonetis, *Genes Dev.* **14**, 278 (2000).

25. Y. Zhang, Y. Xiong, W. G. Yarbrough, *Cell* **92**, 725 (1998).
26. We thank Y. Xu for providing the p53^{L25Q/W265} embryonic stem cells, S. Jones for the p53-MDM2-deficient MEF cells, C. Finlay and T. Kowalik for the MDM2 and p53 adenoviruses, and J. Chen for p53 and HDM2 plasmids. We also thank J. McCarville and G. White Wolf for technical assistance and C. Jenkins for reading the manuscript. Y.Z. is the recipient of a Career Award in Biomedical Science from the Burroughs Wellcome Fund and a Howard Temin Award from National Cancer Institute. Y.X. is the recipient of a Career Development Award from the U.S. Department of Army Breast Cancer Research Program. Supported by NIH grant CA65572 (Y.X.).

27 December 2000; accepted 19 April 2001

In Silico Mapping of Complex Disease-Related Traits in Mice

Andrew Grupe,^{1*} Soren Germer,^{2*} Jonathan Usuka,^{3*} Dee Aud,¹ John K. Belknap,⁴ Robert F. Klein,⁴ Mandeep K. Ahluwalia,² Russell Higuchi,² Gary Peltz^{1†}

Experimental murine genetic models of complex human disease show great potential for understanding human disease pathogenesis. To reduce the time required for analysis of such models from many months down to milliseconds, a computational method for predicting chromosomal regions regulating phenotypic traits and a murine database of single nucleotide polymorphisms were developed. After entry of phenotypic information obtained from inbred mouse strains, the phenotypic and genotypic information is analyzed in silico to predict the chromosomal regions regulating the phenotypic trait.

Identification of genetic susceptibility loci has promised insight into pathophysiologic mechanisms and the development of therapies for common human diseases. Analysis of experimental murine genetic models of human disease biology should greatly facilitate identification of genetic susceptibility loci for common human diseases. We present a computational method that markedly accelerates genetic analysis of murine disease models. A linkage prediction program scans a murine single nucleotide polymorphism (SNP) database and, only on the basis of known inbred strain phenotypes and genotypes, predicts the chromosomal regions that most likely contribute to complex traits. The computational prediction method does not require generation and analysis of experimental intercross progeny, but it correctly predicted the chromosomal regions identified by analysis of ex-

perimental intercross populations for multiple traits analyzed.

A Web-accessible database was developed, which contains allele information across 15 inbred strains and specifies genotyping assays for over 500 SNPs at defined locations in the mouse genome (<http://mouseSNP.roche.com>). These SNPs were identified in our laboratories by direct sequencing of polymerase chain reaction (PCR) amplification products from defined chromosomal locations. This database also incorporates published allele information for 2848 SNPs, 45% of which are characterized in a subset of *Mus musculus* strains; 55% of the SNPs are polymorphic between *Mus castaneus* and one or more *M. musculus* subspecies (1). User queries regarding SNPs found within a specified chromosomal region or between selected inbred strains are executed in real time and provided through a graphical user interface. The oligonucleotide primer sequences and conditions for performing allele-specific kinetic PCR genotyping assays (2) are also provided in the mSNP database [see supplemental material (3)].

To demonstrate the utility of this information, the genome of pooled DNA samples obtained from intercross progeny was analyzed by two different genotyping methods. At 16 weeks of age, the 1000 F₂ progeny of

¹Department of Genetics and Genomics, Roche Bioscience, Palo Alto, CA 94303, USA. ²Roche Molecular Systems, Alameda, CA 94501, USA. ³Department of Chemistry, Stanford University, Stanford, CA 94305-5080, USA. ⁴Oregon Health Sciences University and Portland Veterans Affairs Medical Center, Portland, OR 97201, USA.

*These authors contributed equally to this work.
†To whom correspondence should be addressed: gary.peltz@roche.com